

## Effect of rogue particles on the sub-surface damage of fused silica during grinding/polishing

T. Suratwala<sup>\*</sup>, R. Steele, M.D. Feit, L. Wong, P. Miller, J. Menapace, P. Davis

*Lawrence Livermore National Laboratory, P.O. Box 808, Livermore, CA 94551, USA*

Received 24 May 2007; received in revised form 18 October 2007

Available online 1 February 2008

### Abstract

The distribution and characteristics of surface cracks (i.e., sub-surface damage or scratching) on fused silica formed during grinding/polishing resulting from the addition of rogue particles in the base slurry has been investigated. Fused silica samples (10 cm diameter  $\times$  1 cm thick) were: (1) ground by loose abrasive grinding (alumina particles 9–30  $\mu\text{m}$ ) on a glass lap with the addition of larger alumina particles at various concentrations with mean sizes ranging from 15 to 30  $\mu\text{m}$ , or (2) polished (using 0.5  $\mu\text{m}$  cerium oxide slurry) on various laps (polyurethane pads or pitch) with the addition of larger rogue particles (diamond (4–45  $\mu\text{m}$ ), pitch, dust, or dried Ceria slurry agglomerates) at various concentrations. For the resulting ground samples, the crack distributions of the as-prepared surfaces were determined using a polished taper technique. The crack depth was observed to: (1) increase at small concentrations ( $>10^{-4}$  fraction) of rogue particles; and (2) increase with rogue particle concentration to crack depths consistent with that observed when grinding with particles the size of the rogue particles alone. For the polished samples, which were subsequently etched in  $\text{HF}:\text{NH}_4\text{F}$  to expose the surface damage, the resulting scratch properties (type, number density, width, and length) were characterized. The number density of scratches increased exponentially with the size of the rogue diamond at a fixed rogue diamond concentration suggesting that larger particles are more likely to lead to scratching. The length of the scratch was found to increase with rogue particle size, increase with lap viscosity, and decrease with applied load. At high diamond concentrations, the type of scratch transitioned from brittle to ductile and the length of the scratches dramatically increased and extended to the edge of the optic. The observed trends can be explained semi-quantitatively in terms of the time needed for a rogue particle to penetrate into a viscoelastic lap. The results of this study provide useful insights and ‘rules-of-thumb’ relating scratch characteristics observed on surfaces during optical glass fabrication to the characteristics of the rogue particles causing them and their possible source.

Published by Elsevier B.V.

PACS: 42.86.+b; 81.40.Np; 46.55.+d

Keywords: Fracture; Indentation, microindentation; Optical microscopy; Lasers; Silica; Processing

### 1. Introduction

The creation of sub-surface mechanical damage (SSD) (i.e., surface micro-cracks) can be thought of as the repeated indentation of mechanically loaded hard indenters (abrasives) sliding on the surface of a brittle substrate (workpiece) during various cutting and grinding processes. These surface cracks are commonly identified as scratches

and digs. During grinding operations, the removal of material is governed by the intersection of multiple surface cracks.

For static indents, the loads needed to initiate fracture (lateral, radial, Hertzian) are finite and can be analytically expressed in terms of the size of particle for blunt indentors and material properties for sharp indentors [4]. The critical load for a sharp indenter to create fracture in fused silica is  $\sim 0.02$  N [4]. For sliding indents (i.e., leading to scratching), the types of features (trailing indent cracks, median cracks, lateral cracks, and plastic deformation/compaction) [4,9,10]

<sup>\*</sup> Corresponding author. Tel.: +1 925 422 1884; fax: +1 925 423 0792.

E-mail address: [suratwala1@llnl.gov](mailto:suratwala1@llnl.gov) (T. Suratwala).

are a function of the local shape of the particle at contact (sharp vs blunt) and the applied load. At low loads ( $P < 0.05$  N) a plastic trench is formed without fractures. At intermediate loads ( $0.1 \text{ N} < P < 5 \text{ N}$ ) well defined radial (or trailing indent) fractures along with lateral cracks are observed. At higher loads ( $P > 5 \text{ N}$ ), the plastically deformed track fractures into a rubble-like appearance, and lateral and trailing indent cracks are less pronounced.

In contrast, the general material removal mechanism responsible for polishing is less straightforward. Various mechanisms have been proposed including surface melting [1], plastic removal or abrasion [2,3], brittle fracture [4,5], adhesion [6], and chemical [2]. However, the most widely accepted mechanism involves the removal of material by a chemical reaction between the polishing particle and the substrate resulting in molecular level removal [2,5,7,8].

One aspect of the transition from grinding to polishing can be thought of in terms of the decrease in particle size of the slurry and the subsequent decrease in the load/particle. During grinding larger particles are used (greater than  $\sim 10 \mu\text{m}$ ), resulting in fewer loaded particles per unit area between the workpiece and the lap and thus, resulting in loads/particle that exceed the initiation load for fracture. During polishing smaller particles are used (less than  $3 \mu\text{m}$ ), resulting in more loaded particles per unit area and loads/particle below the fracture initiation load. For a typical ceria based polishing slurry ( $0.5 \mu\text{m}$ ), assuming a 0.3 fill fraction at the interface and all the particles are load bearing, one estimates a load/particle of  $10^{-9}$ – $10^{-6}$  N. Clearly, the load on an average polishing particle is many orders of magnitude lower than needed to initiate fracture. Thus any scratch formed on a polished surface implies a particle (i.e. a larger (rogue) particle) that is holding a much higher load than the average particle.

The presence of rogue (i.e. large) particles in the slurry during grinding or polishing is known to strongly influence surface properties of the workpiece either in terms of deeper damage or isolated scratching [2,4,11]. Several studies for polishing integrated circuits have investigated the effects of rogue particles for wafers ground or polished using chemical mechanical polishing. Basim et al. [12] spiked colloidal silica slurries with rogue silica particles and found that scratch densities increased with rogue particle size and concentration. By characterizing the slurry size distribution using dynamic light scattering, Basim also illustrated that rogue particles present even at a very low concentration ( $< 1$  out 100 000) can degrade surface quality. Ahn et al. [11] and Kallingal et al. [13] compared different colloidal silica and colloidal alumina based slurries of different pH, filtering, or ultrasonic preparation to reduce micro-scratches; the results were explained in terms of how the process parameters affect the large particles in the distribution.

In our previous studies, the characteristics and statistical distribution of SSD as a function of different grinding processes using a polished taper technique have been measured and analyzed [14–16]. These results suggested that only a

small fraction (1 out of tens of thousands of particles) of the abrasive particles were participating in the material removal by comparing the measured crack depth with that expected from static indentation models. Hence only a small fraction of the particles were being mechanically loaded. In the present study, the effects of rogue particle additions during both grinding and polishing and their effect on the SSD depth and the characteristics of scratching have been investigated. Understanding the impact of the presence of rogue particles during grinding and polishing can ultimately be used to develop finishing processes resulting in minimal or no SSD. This is important in areas which require high quality polished brittle surfaces including integrated circuits, high strength windows, and optics for use in high power laser applications [17].

## 2. Experimental

### 2.1. Ground samples

Round fused silica samples (10 cm diameter  $\times$  1.0 cm thick) were ground or polished using slurries that were intentionally contaminated with various concentrations and sizes of rogue particles. Ground samples were prepared on a rotary 8" borosilicate glass lap (0.3 psi, 1 h, 15 rpm lap) using an alumina abrasive particle (Microgrit 9T or 15T) slurry. Rogue particles (Microgrit 15T or 30T) were added to the base slurry at various concentrations. The SSD distributions of the as-prepared surfaces were then determined by: (1) creating a shallow (10–100  $\mu\text{m}$ ) wedge/taper on the surface by magneto-rheological finishing; (2) exposing the SSD by HF/NH<sub>4</sub>F acid etching; and (3) performing image analysis of the observed cracks from optical micrographs (Nikon Optiphot, reflectance) taken along the surface taper (see Fig. 1). Details of this characterization technique to determine SSD depth and length distributions are provided elsewhere [14–16]. Photographs of the grinding setup is shown in Fig. 2(a) and the particle size distributions of the loose abrasives used in the rogue particle experiments are shown in Fig. 3(a). The matrix of experiments for the ground samples are shown in Table 1.

### 2.2. Polished samples

The pitch lap was prepared by heating 500 g of Gugolz 73 ground in  $\sim$ mm sized pieces in an aluminum foil covered stainless steel container (12 cm diameter  $\times$  16 cm) in a convection oven at 76.7 °C for 60 min. The pitch was stirred after 30 min and 50 min. The molten pitch was then poured immediately after removal from the oven onto a preheated (76.7 °C) aluminum plate block (20 cm diam) with tape (3M black duct) wrapped around the edge on a flat, level surface until the lap formed the desired thickness. After 10 min, that tape was removed and the groove pattern (3.8 cm triangles with 3 mm wide, 3 mm deep, 60° V-grooves) was embossed using a rubber mask. The embossing was accomplished by placing the mask on the

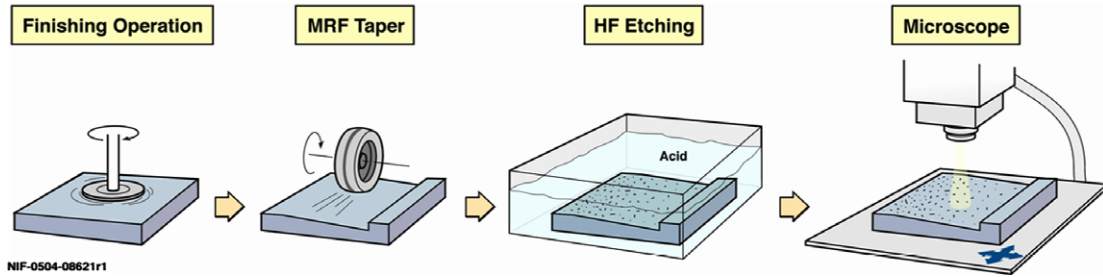


Fig. 1. Schematic illustrating the steps in the wedge technique to determine SSD depth distributions.

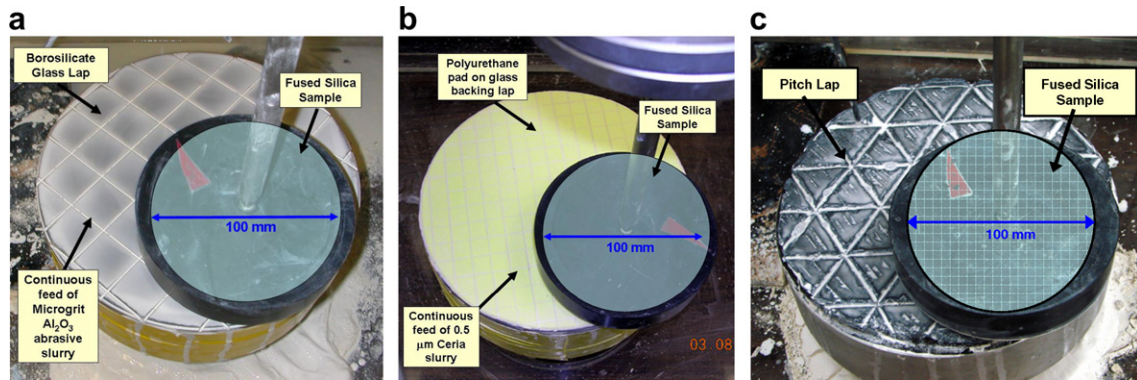


Fig. 2. Photos of the (a) grinding and (b) and (c) polishing setups.

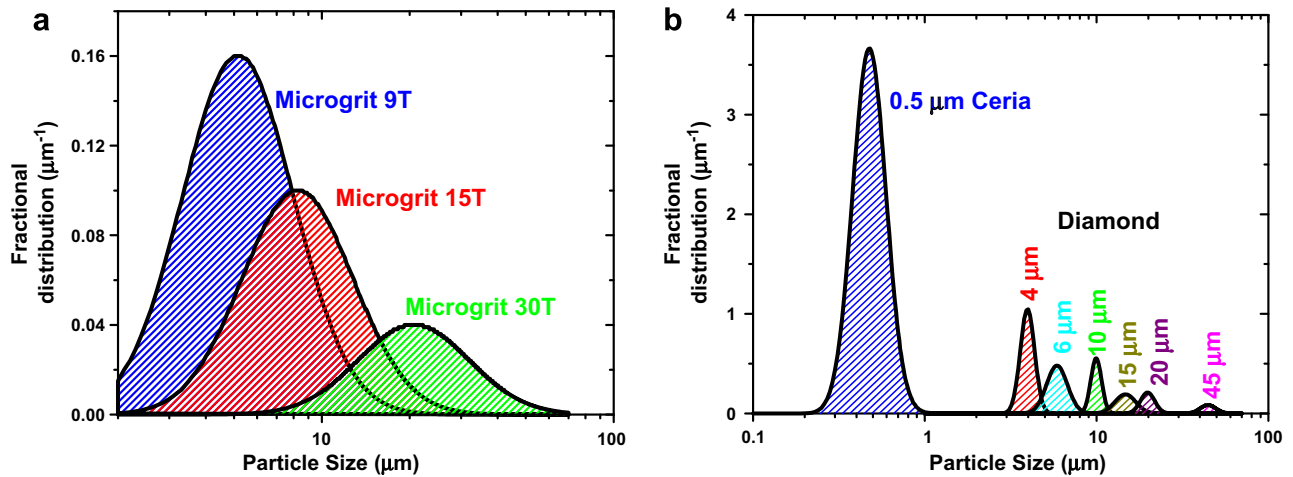


Fig. 3. (a) Particle size distributions of the  $\text{Al}_2\text{O}_3$  slurry used in the grinding experiments; and (b) particle size distributions of the cerium oxide slurry and rogue diamond particles added during the polishing experiments. Data from manufacturer literature.

pitch and rotating the lap upside down on the flat, level surface for 3 min. The polyurethane lap (Suba 550) was prepared by adhering the lap material on a glass substrate and by routing 1 mm grooves in a 10 square pattern. Figs. 2(b) and (c) show photos of the polishing laps.

Polished samples were prepared by first removing all the pre-existing SSD by ceria polishing on an 8" rotary polisher using Hastilite PO ceria slurry on a polyurethane pad (0.3 psi, 15 rpm lap) (Suba 550) or on pitch (Gugolz 73). The SSD damage removal was verified by HF/ $\text{NH}_4\text{F}$  etch-

ing for 30 min and inspecting the surface by optical microscopy for any observable surface cracks.

The fused silica samples were then repolished for 1 h with the same polishing slurry contaminated: (1) at various abrasive sizes of 4, 6, 10, 15, 20 or 45  $\mu\text{m}$  at various concentrations using rogue diamond particles (Diamond Innovations DMS Poly 285T) on the polyurethane pad, (2) at various loads using 6  $\mu\text{m}$  diamond on polyurethane pad, (3) on various laps using the 6  $\mu\text{m}$  diamond, (4) at various temperatures using 6  $\mu\text{m}$  diamond on pitch, and (5) with

Table 1  
Summary of results from rogue particle addition during Al<sub>2</sub>O<sub>3</sub> loose abrasive grinding on a glass lap

Sample	Base particle size (μm)	Rogue particle size (μm)	Weight % rogue particles	Rogue particle areal density (#/cm <sup>2</sup> )	Rogue particle fraction (by number)	Removal rate SSD depth (μm/h)	Mean crack length (μm)	Weighted roughness (μm)	PV roughness (μm)	Average load/particle (N)	Surface density (×10 <sup>5</sup> cm <sup>-2</sup> )	Maximum crack length (μm)
(a)	(a)	(a)	±15%	(b)	±15%	±1.5%	(c)	(d)	(d)	(e)	(e)	(e)
G1	9	–	–	–	–	6	2.0	0.4	1.4	8 × 10 <sup>-5</sup>	–	68
G2	15	–	–	–	–	64	3.8	0.9	4.2	0.006	50	80
G3	30	–	–	–	–	130	15.5	2.0	8.5	0.003	12	190
G4	9	15	0.1	100	2 × 10 <sup>-4</sup>	45	5.8	0.6	2.0	0.001	200	95
G5	15	30	0.001	0.2	1.3 × 10 <sup>-6</sup>	72	7.9	0.7	4.0	0.001	17	150
G6	15	30	0.01	2	1.3 × 10 <sup>-5</sup>	63	7.9	0.8	5.0	0.0006	40	160
G7	15	30	0.1	20	1.3 × 10 <sup>-4</sup>	69	7.4	0.7	3.8	0.004	70	100
G8	15	30	1	200	1.3 × 10 <sup>-3</sup>	74	7.1	0.8	4.8	0.002	20	150
G9	15	30	50	15000	0.14	98	14.6	1.5	7.5	0.001	5	210

(a) Particle size distribution of the loose abrasive are shown in Fig. 3(a) as reported by manufacturer. (b) Values are approximate and relative assuming all particles are of mean size and only a monolayer of particles are at interface. (d) Crack length distributions are shown in Fig. 5(b) and (d). (c) Values calculated from profilometry data (see ref [14] for details). (e) Values determined as fitting parameters from best fit crack depth and length distribution data shown in Fig. 5 to grinding model described in Ref. [14].

various types of rogue particles (dust, diamond, pitch, dried ceria) on pitch. The matrix of experiments for the polishing experiments is shown in Table 2.

The morphology of the diamond particles was examined by scanning electron microscopy. The characteristics of the resulting scratches due to the rogue particles were then characterized by optical microscopy after HF/NH<sub>4</sub>F etching to expose all the SSD. Note all the crack features were observable by optical microscopy only after etching. The particle size distributions of the rogue particles used in the polishing experiments are shown in Fig. 3(b).

### 3. Results

#### 3.1. Rogue particles during grinding

Table 1 shows the basic experimental parameters and a summary of the results for the ground samples (G1–G9). The removal rate, measured SSD depth, average crack length, surface roughness and the calculated average load/particle, surface density of cracks, and the maximum crack length for each of the samples are listed. The last three parameters are calculated using a brittle fracture model described in detail in our previous study [14].

The number density of cracks on a typical ground surface is very high, such that the individual cracks intersect each other giving a rubble-like appearance. However, a few microns below the surface (i.e. after polishing through it), one can now identify distinct individual cracks, all of a common morphology, which decrease in number density with depth. Most of these cracks have a ‘trailing indent’ character [14] (commonly referred to as chatter marks [18] or stick-dig fractures). Fig. 4 shows an optical micrograph of a ground surface after the rubble-like surface has been removed, illustrating the typical individual cracks observed on a ground surface. The length or size of these trailing indents cracks have been found to scale with the size of the abrasive particle used for grinding [14,16]. Note that both the width and length of the original cracks have increased in size by ~1 μm due to the etch process opening up the cracks.

Fig. 5(a) and (c) shows the SSD depth distributions measured by the taper polish technique on the series of loose abrasive ground surfaces with various concentrations of rogue particle additions to the slurry. The crack depth distributions are reported in terms of cumulative crack obscuration (crack area fraction) as a function of depth into the original treated glass surface. Obscuration was used instead of crack number density to describe the SSD density because the intersection of cracks near the surface causes a significant uncertainty in the crack number density. The shape of the depth distributions follows a single exponential dependence for the majority of the distribution except near the end of the distribution where crack density drops very rapidly, appearing like an asymptotic cutoff. Depth distributions measured in our previous study also show this behavior [14]. The SSD depth was observed to increase

Table 2  
Summary of results from rogue particle addition during 0.5 CeO<sub>2</sub> polishing on a polyurethane pad or pitch

Sample	Rogue particle	Rogue particle size	Rogue particle areal density	Pressure	Temperature	Pad material	Scratch number density	Average scratch length	Average scratch width	Scratch type		
		( $\mu\text{m}$ )	( $\#/\text{cm}^2$ )	(psi)	( $^{\circ}\text{C}$ )		( $\#/\text{cm}^2$ )	( $\mu\text{m}$ )	( $\mu\text{m}$ )	Brittle (%)	Plastic + Brittle (%)	Plastic (%)
		(a)	(b)	<1%	$\pm 0.1$	na	<5%	(c)	$\pm 50\%$ (d)	$\pm 3\%$	$\pm 3\%$	$\pm 3\%$
P1	–	–	0	0.3	23.8	PU	0	–	–	–	–	–
P2	Diamond	4	5	0.3	23.8	PU	0.5	475	2.1	61	28	11
P3	Diamond	4	50	0.3	23.8	PU	1.6	336	2.1	55	43	2
P4	Diamond	4	500	0.3	23.8	PU	1.0	409	1.8	54	43	3
P5	Diamond	4	5000	0.3	23.8	PU	98	Across optic	10	1	0	99
P6	Diamond	6	50	0.3	23.8	PU	7.2	585	2	96	0	4
P7	Diamond	10	50	0.3	23.8	PU	2.0	867	3.5	44	47	9
P8	Diamond	15	50	0.3	23.8	PU	2.9	839	3.3	48	24	27
P9	Diamond	20	50	0.3	23.8	PU	25	1310	2.8	56	16	28
P10	Diamond	45	50	0.3	23.8	PU	3000	Across optic	12	0	20	80
P11	Diamond	6	50	0.1	23.8	pitch	3500	13,500	0.7	0	100	0
P12	Diamond	6	50	0.3	23.8	pitch	1.4	2160	5	80	20	0
P13	Diamond	6	50	1.5	23.8	pitch	24	430	1.9	61	18	21
P14	Diamond	6	50	0.3	23.8	IC1000	1.5	1350	1	0	43	57
P15	Diamond	6	50	0.3	27.7	pitch	0.6	1680	5	29	29	41
P16	Diamond	6	50	0.3	31.6	pitch	0.9	1100	3	43	43	14
P17	ASTM Urban dust	13	10,000	0.3	23.8	pitch	0	–	–	–	–	–
P18	Pitch	20*	1600	0.3	23.8	pitch	34	2160	4	29	62	7
P19	Dried ceria	45	3300	0.3	23.8	pitch	7	2539	3	70	30	0

(a) Size distributions for the diamond particles are shown in Fig. 3(b) as reported by manufacturer. (b) Values are approximate and relative assuming all particles are of mean size and only a monolayer of particles are at interface. (c) A distribution of scratch lengths were measured; the measured scratch length distributions are shown in Fig. 11. (d) A distribution of crack widths were measured from a minimum of 20 scratches (typically 50) per sample; typical 1 sigma in the distribution is reported. RT = room temperature, uncontrolled; PU = polyurethane pad; \*Pitch particle has a large aspect ratio measured average was  $20 \mu\text{m} \times 80 \mu\text{m}$ .

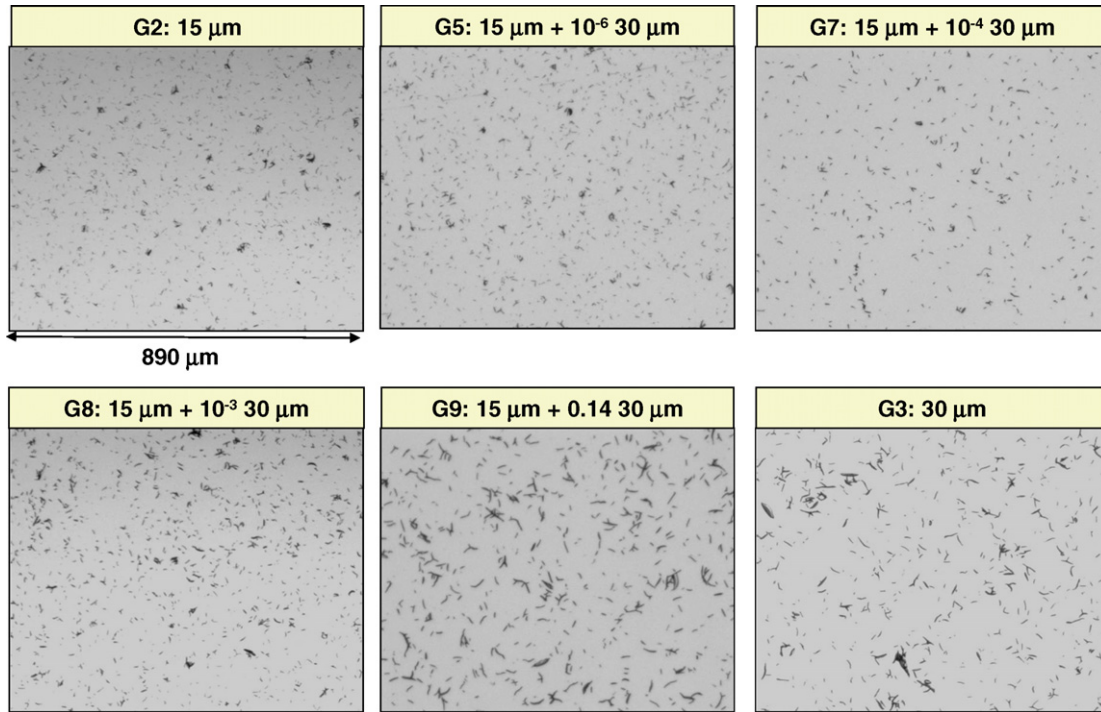


Fig. 4. Microscope images of the trailing indent cracks observed on the ground samples prepared with 15  $\mu\text{m}$  and 30  $\mu\text{m}$  loose abrasives and various mixtures. The images were taken along the wedge of the sample (i.e. representative of the crack density just below the surface).

significantly even with a small amount of rogue particles for both the 9  $\mu\text{m}$  plus 15  $\mu\text{m}$  rogue particles (Fig. 5(a)) and 15  $\mu\text{m}$  plus 30  $\mu\text{m}$  rogue particles (Fig. 5(c)) series samples.

The corresponding crack cumulative crack length distribution for the same set of samples is shown in Fig. 5(b) and (d). From our previous studies [14], the length of the trailing indent fracture was found to be correlated directly to the size of the abrasive leading to fracture. As shown in Table 1, the average crack length for the 15  $\mu\text{m}$  loose abrasive (G2) was 3.8  $\mu\text{m}$  and for the 30  $\mu\text{m}$  loose abrasive was 15.2  $\mu\text{m}$ . Upon examination of Fig. 5(b) and (d), the crack length distribution shifted to larger values with an increase in rogue particle concentration and approached that of the size of the trailing indent crack expected for the rogue particle itself. This suggests that with increasing rogue particle concentrations, the rogue particles were participating more in causing fracture. This is also consistent with the crack depth distributions data discussed above.

Fig. 6(a) shows a plot of the maximum SSD observed as a function of the rogue particle concentration. The horizontal dashed lines illustrate the bounds by which the SSD depth was observed with the base particle slurry alone and with the rogue particle slurry alone. The measured SSD depth with the rogue particles are bound by these limits which is not a surprising result. However, it appears that the SSD depth will start to increase from the depth found with the base slurry at a fairly low fraction of rogue particles ( $<10^{-4}$ ) or at an areal density of  $10\text{ cm}^{-2}$ . Hence only a small amount of rogue particles is enough to increase the SSD. Interestingly, the removal rate also starts to notice-

ably increase with the addition of rogue particles somewhere between  $10^{-3}$  and  $10^{-4}$  fraction of rogue particles and start to approach the removal rate of the rogue particle alone (see Fig. 6(b)).

### 3.2. Rogue particles during polishing

Table 2 shows basic experimental parameters and a summary of the results for the polished samples (P1–P19). The results include the observed scratch properties (the number density, average length, average width, and the percentage of the types of scratches observed). Without the addition of rogue diamond particles during polishing (i.e., only using a slurry made from Hastilite PO Cerium oxide), our polisher was able to repeatedly create surfaces that showed no scratches or digs after etching the sample (e.g., sample P1). Note that before any of the other polishing samples (P2–P19) were prepared, all the scratches and digs were removed from each substrate using the same procedure as noted for P1 (i.e., without rogue particles) to ensure that the observed scratches were caused by the rogue particles that were added to the slurry.

The various types of scratches that were observed as a result of the addition of rogue particles are shown in Fig. 7. These scratches can be divided into three basic categories: (1) Plastic which are scratches that show no brittle fracture but just plastic modification to the surface (often referred to as sleeks); (2) Brittle which are scratches that have only cracks (trailing indent or lateral); and (3) Mixed which are scratches that contain both plastic modification and cracks. The scratches can then be further categorized

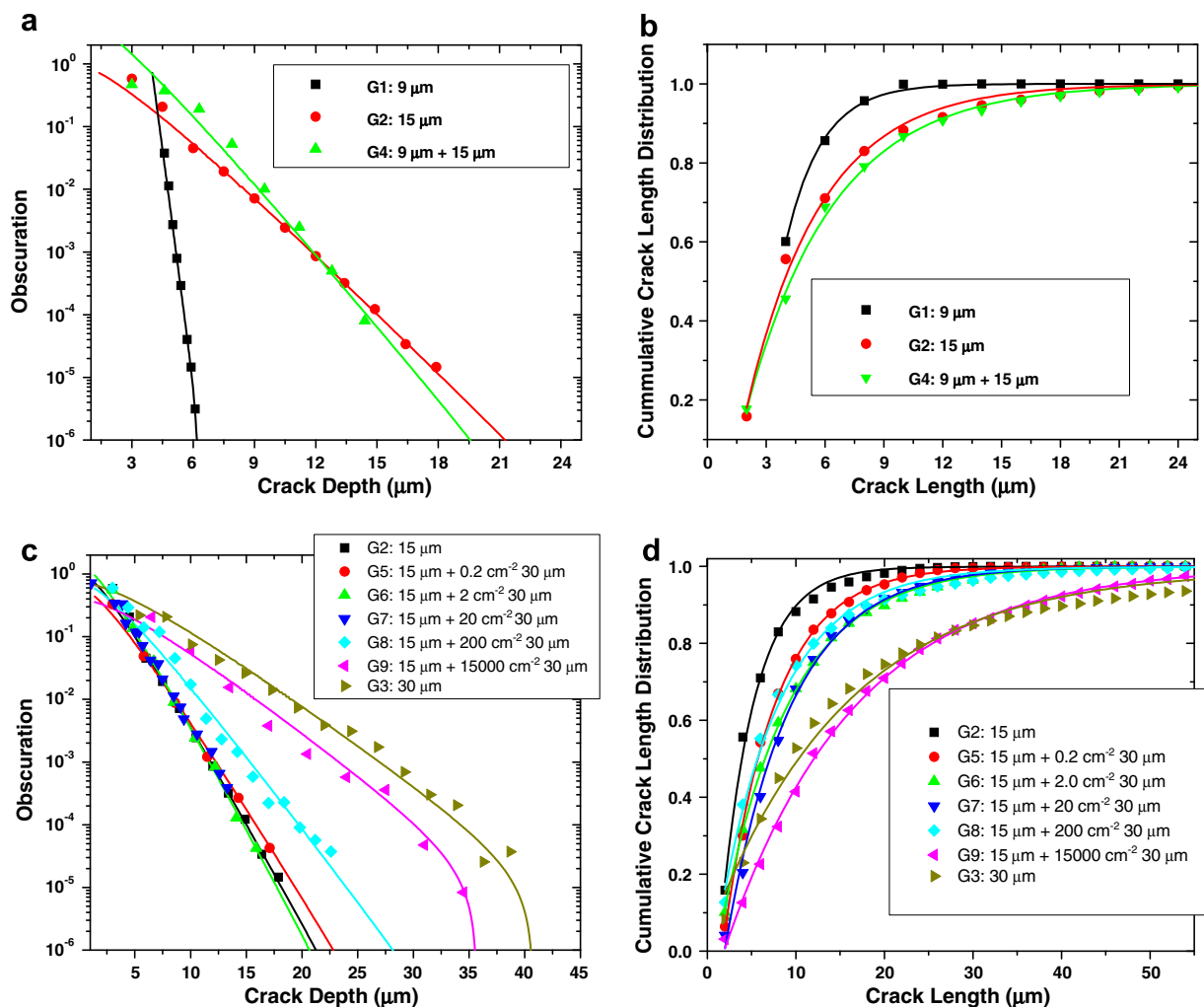


Fig. 5. (a) SSD depth distribution and (b) crack length distribution of the fused silica surface after loose abrasive grinding with 9  $\mu\text{m}$ , 15  $\mu\text{m}$ , and 9  $\mu\text{m}$  contaminated with 15  $\mu\text{m}$  alumina particles; (c) SSD depth distribution and (d) crack length distribution of the fused silica surface after loose abrasive grinding using 15  $\mu\text{m}$ , 30  $\mu\text{m}$ , and 15  $\mu\text{m}$  contaminated with 30  $\mu\text{m}$  alumina particles. The lines are curve fits using the model described in Ref. [14].

by the types of cracks (lateral or trailing indent). Plastic type scratches would be expected from sharp indenters where the local pressure exceeds the yield stress at the contact zone. Purely brittle type scratches would be expected from blunt type indenters. Scanning electron microscope images of the diamond rogue particles ranging from 4 to 45  $\mu\text{m}$  are shown in Fig. 8, which show that the diamond particles have both a blunt and sharp character to them; thus, it is not surprising that both plastic and brittle scratches were observed.

The scratch dimensions (length, width) and the scratch number density as functions of rogue particle size and rogue particle diamond concentration are summarized in Fig. 9(a)–(d). The scratch number density was found to increase exponentially with rogue particle size at a fixed rogue particle number concentration (see Fig. 9(a)). This suggests that the larger the rogue particle, the greater the probability or the more efficient it is in causing scratches. The magnitude of the difference in scratch number density with particle size is also illustrated in the microscope images shown in Fig. 10. Interestingly, the scratch number density was much less

sensitive to the rogue particle concentration. For most of the rogue particle concentrations examined (5–500  $\text{cm}^{-2}$ ) the scratch concentration did not change by more than a factor of 5. However, at very high rogue particle concentration (5000  $\text{cm}^{-2}$ ), the plastic scratch number density increased by a factor of 1000 (see Fig. 9(b)).

The width and the length of the scratches were both observed to increase with rogue particle size and were relatively insensitive to rogue particle concentration except at very high rogue particle concentration (Fig. 9(c)–(d)). The width increase is attributed to the larger contact zone expected with larger rogue particles; the width of the scratch was nominally 15–30% of the mean diamond diameter added to the slurry. The scratch length was also noted to increase with diamond particle size in the range of 4–20  $\mu\text{m}$  (Fig. 9(c)). Fig. 11(a) illustrates this trend more definitively by plotting the cumulative scratch length distribution observed for various rogue diamond particles. A similar plot (Fig. 11(b)) shows the effect of pitch temperature on the scratch length distribution, whose results will be discussed in more detail in the Section 4.

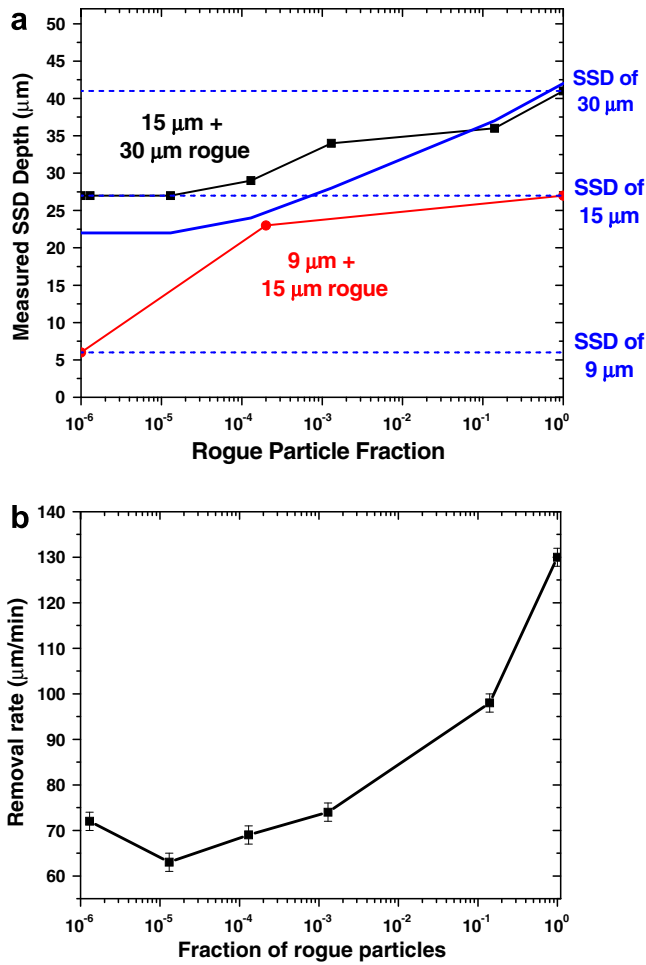


Fig. 6. (a) Maximum SSD depth as a function of rogue particle concentration (of 15  $\mu\text{m}$  or 30  $\mu\text{m}$  alumina relative to the SSD observed on the 9  $\mu\text{m}$  and 15  $\mu\text{m}$  loose abrasive grinding without the addition of rogue particles. The solid line without data points represents the model described by Eqs. (8) and (9) in Section 4.1. (b) Measured removal rate of the 15  $\mu\text{m}$  loose abrasive grinding as a function of the rogue 30  $\mu\text{m}$  concentration.

Rogue particles of different material types were shown to cause scratches. Whether the rogue particles were diamond (P12), pitch particles (P18), or dried ceria agglomerates (P19), scratches were created (see Table 2). The only exception was organic urban dust (P17) which did not lead to any measurable SSD. Pitch particles and dried ceria agglomerates are common sources of rogue particles during polishing, and these results confirm that cleanliness and the elimination of pitch particle sources and dried slurry around the polisher are critical to obtain scratch-free surfaces.

## 4. Discussion

### 4.1. Rogue particles during grinding and load/particle

The change in the SSD depth distribution with the addition of rogue particles during grinding can be rationalized in terms of the change in the particle size distribution which leads to a change in the load distribution of particles in

contact with the workpiece. In our previous study [14], a brittle fracture model was used to describe how the particle size distribution of the grinding particles leads to the crack depth and length distributions. Some of the key features of the model include: (1) only the larger particles in the distribution are loaded and lead to fractures; and (2) the load on a given particle scales linearly with the size of the particle. Using this brittle fracture model as a basis, one can gain insight to the behavior observed when two particle size distributions are mixed. For this analysis, assume that the particles (both the base and the rogue) have a log-normal distribution ( $g(d)$ ) in the form:

$$g(d) = \frac{1}{d\sqrt{2\pi\ln\sigma}} e^{-\frac{(\ln(d)-\ln(d_c))^2}{2\ln\sigma^2}}, \quad (1)$$

where  $d$  is the size of the particle,  $\sigma$  is a parameter that describes the width of the distribution, and  $d_c$  is the mean particle size. When the two particles distributions are mixed, the resulting distribution ( $g_r(d)$ ) is simply the geometric sum of the two given by:

$$g_r(d) = (1 - x_r)g_b(d) + x_r g_r(d), \quad (2)$$

where  $g_b(d)$  is the base particle size distribution,  $g_r(d)$  is the rogue particle size distribution, and  $x_r$  is the number fraction of particles from the rogue particle size distribution. Then the fraction of particles being loaded and resulting in SSD is given by:

$$f_{\text{load}} = \int_{d_{\min}}^{d_{\max}} g_r(d) \partial d, \quad (3)$$

where  $d_{\min}$  is the minimum particle size that is mechanically loaded and participates in the fracture and  $d_{\max}$  is the largest particle size in the distribution. For simplicity, assume that the fraction of particles being loaded is the same regardless of the mixture of the two distributions. Knowing  $f_{\text{load}}$ , one can determine  $d_{\min}$  numerically; in order words, one now knows the distribution of loaded particles.

Using an analysis utilized in the previously described model [14], the loaded particle distribution can be then converted to a fractional distribution of crack depths ( $f_c(c)$ ) and cumulative obscuration or crack density depth distribution ( $O(c)$ ), which are given by:

$$f_c(c) = g_r(d) \frac{\partial d}{\partial c}, \quad (4)$$

$$O(c) = \int_c^{c_{\max}} f_c(c) w n L(c) dc. \quad (5)$$

Substituting values for  $\partial d/\partial c$  and  $L(c)$  as derived in the previous study as:

$$\frac{\partial d}{\partial c} = \frac{3}{4} \left( \frac{K_{Ic} N_L d_c^2}{\chi_h P_T} \right)^{1/2} c^{-1/4}, \quad (6)$$

$$L(c) = \frac{\pi}{2} \left( \frac{K_{Ic} N_L d_c^2}{\chi_h P_T} \right)^{1/2} \left( \frac{2kP_T}{3EN_L d_c^2} \right)^{1/3} c^{3/4} \quad (7)$$

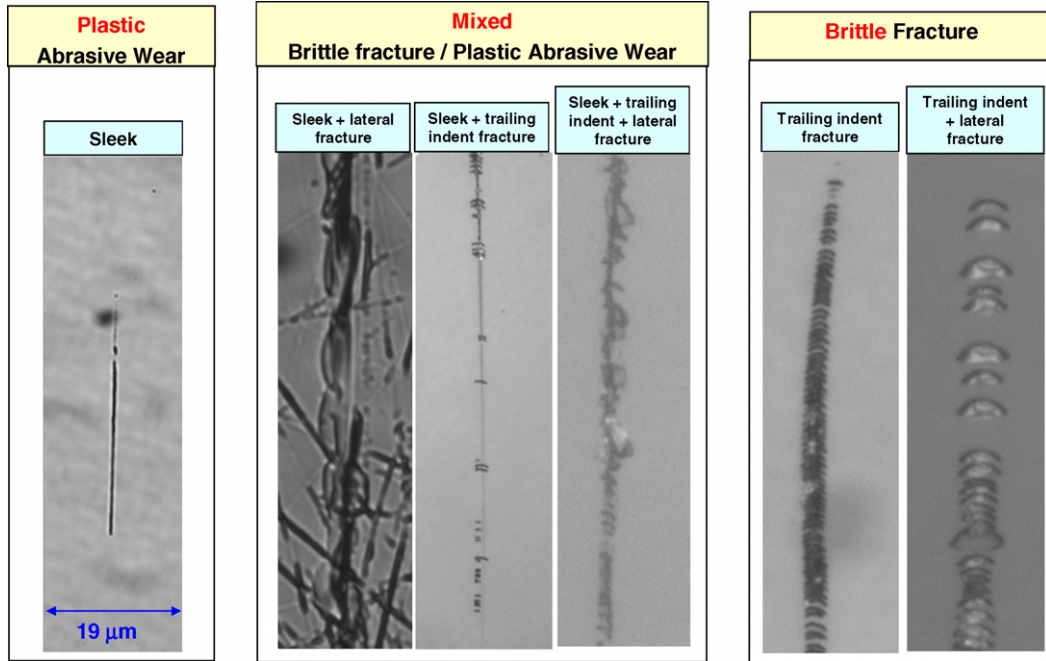


Fig. 7. Categories of different type of scratches observed in samples P1–P19.

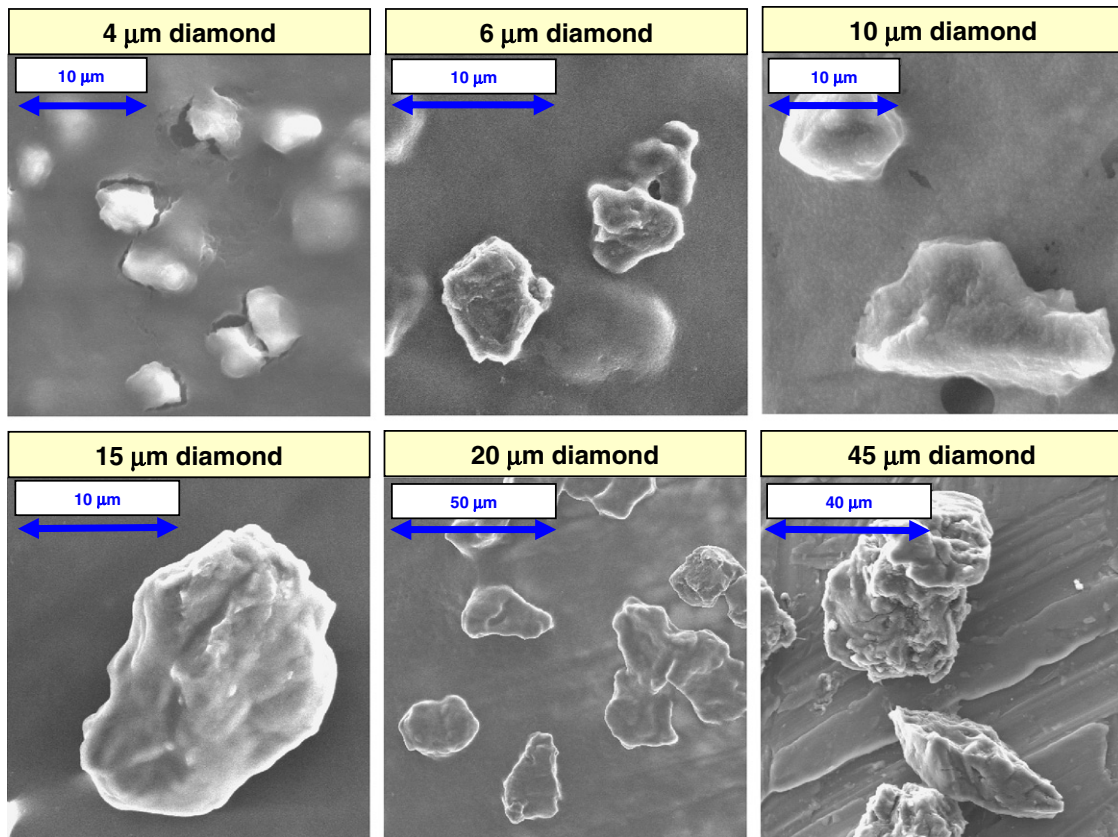


Fig. 8. SEM images of diamond particles used as the rogue particles for samples P2–P10.

and simplifying, the following expression for the crack depth distribution is obtained:

$$O(c) = \int_c^{c_{\max}} g_t(d)c^{1/2}Qdc, \tag{8}$$

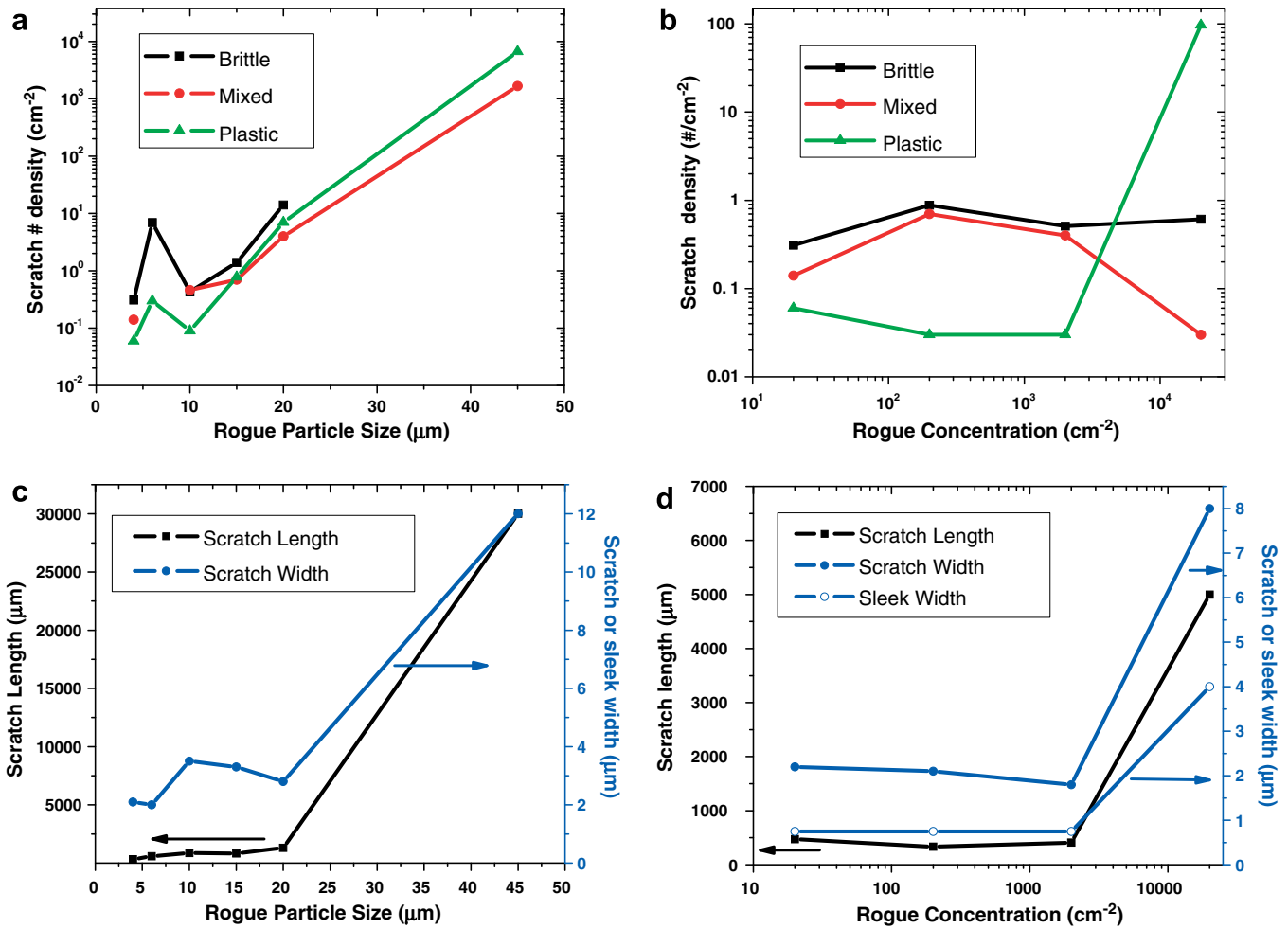


Fig. 9. Scratch number density observed after ceria polishing of fused silica with rogue diamond particle addition as a function of: (a) rogue particle size at a fixed rogue particle concentration of  $50 \text{ cm}^{-2}$  and (b) rogue particle concentration at a fixed rogue particle size of  $4 \text{ }\mu\text{m}$ . Scratch dimensions (length, width) observed after ceria polishing of fused silica with rogue diamond particle addition as a function of: (c) rogue particle size at a fixed rogue particle concentration of  $50 \text{ cm}^{-2}$  and (d) rogue particle concentration at a fixed rogue particle size of  $4 \text{ }\mu\text{m}$ . The data are from samples P2–P10 described in Table 2.

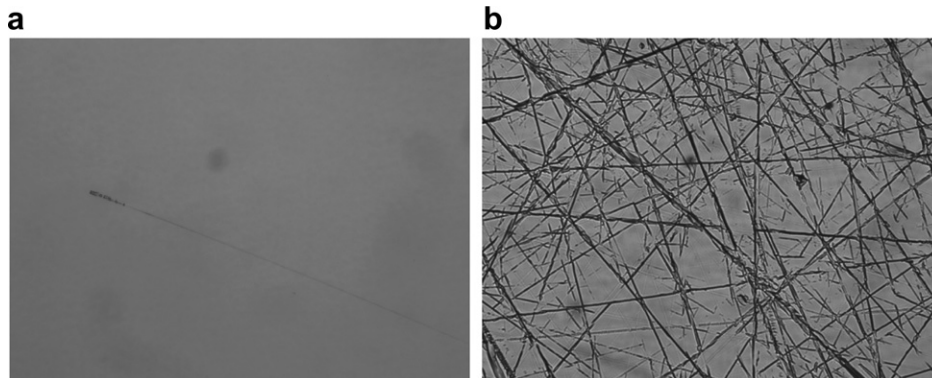


Fig. 10. (a) Typical scratch observed on a polished surface upon addition of  $10 \text{ }\mu\text{m}$  diamond particles (P2) (b) Typical scratches observed on a polished surface upon the addition of  $45 \text{ }\mu\text{m}$  diamond particles (P10). The horizontal full scale on each image is  $237 \text{ }\mu\text{m}$ .

where  $Q$  is:

$$Q = \frac{3\pi K_{Ic} w n}{8\chi_h} \left( \frac{N_L d_c^2}{P_T} \right)^{2/3} \left( \frac{2k}{3E} \right)^{1/3}, \quad (9)$$

where  $K_{Ic}$  is the fracture toughness of the substrate,  $N_L$  is the number of abrasive particles being loaded,  $d_c$  is the mean abrasive particle size,  $\chi_h$  is the Hertzian indent crack growth constant,  $P_T$  is the applied load,  $w$  is the width of

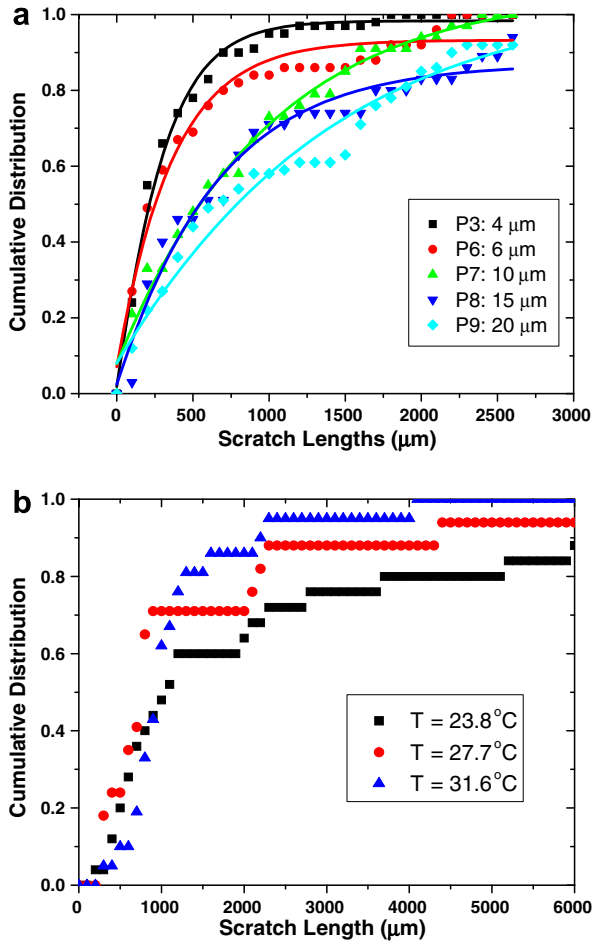


Fig. 11. (a) Cumulative scratch length distribution measured for ceria polished samples with rogue particles of different sizes and a constant rogue diamond concentration of  $50 \text{ cm}^{-2}$ . The average crack lengths determined from these distributions are reported in Fig. 9(c). (b) Effect of pitch temperature on the scratch length distribution during pitch polishing with  $0.5 \mu\text{m}$  Ceria and  $6 \mu\text{m}$  rogue diamonds at  $50 \text{ cm}^{-2}$  concentration.

the crack on surface,  $n$  is the number density of cracks on the surface, and  $k$  is material constant related to the modulus and Poisson's ratio of the substrate and indenter.

Using Eqs. (1)–(3), the loaded distribution of particles as a function of rogue particle concentration has been calculated. By taking the simple case where the fraction of particles being loaded ( $f_L \sim 0.01$ ), the number density of cracks on the surface ( $n \sim 0.05 \mu\text{m}^{-2}$ ), and the load for the average loaded particle ( $P_T/N_L \sim 0.25 \text{ N}$ ) do not change with the addition of rogue particles, we can estimate the SSD depth predicted by Eqs. (1)–(9). The calculated SSD is reported in Fig. 6(a) by the solid line. The assumptions described above are likely an oversimplification of the real system. However, this simple model predicts SSD depths that are consistent with measured data as a function of the rogue particle concentration. This model can be used to estimate the SSD depth in the presence of rogue particles or as a method to estimate the size or concentration of rogue particles based on an observed change in SSD depth distribution.

#### 4.2. Scratch characteristics and viscoelastic model

During an ideal polishing process (as opposed to grinding), material removal occurs chemically at the molecular level rather than by mechanical fracture [2]. During polishing, the nominal load per polishing particle is quite low ( $10^{-9}$ – $10^{-6} \text{ N}$ ), well below that needed to initiate fracture [2]. However, when rogue particles are present during polishing, the mechanical load on the rogue particle can be orders of magnitude higher, resulting in a rogue particle-induced fracture (i.e., scratching). Loads on the order of  $0.001 \text{ N}$  for plastic and  $0.1 \text{ N}$  for brittle fracture initiation are needed [4,9]. The addition of rogue diamond particles lead to surface scratches whose width, length and number density depend on the size and concentration of the rogue particles added.

As discussed in Section 3.2, there are three major trends that were observed: (1) the propensity of rogue particles to lead to scratches is strongly dependent on the size of the rogue particle and weakly dependent on the concentration; (2) the length and width of the scratches both increase with the size of the rogue particle and are essentially independent of concentration; (3) at the highest rogue diamond size ( $45 \mu\text{m}$ ) and at the very high rogue diamond concentrations for the  $4 \mu\text{m}$  diamond, the number density of scratches increases by orders of magnitude, the scratch lengths are the length of the optic (quasi infinite), and the nature of the scratches were all plastic in nature. The discussion below describes a model to explain the latter two observations.

The mean scratch lengths increased from  $\sim 330$  to  $\sim 1300 \mu\text{m}$  with rogue particle size (see Table 2 and Fig. 11). For these samples, the scratch number densities were  $\sim 2$ – $25 \text{ cm}^{-2}$  or nominally 150–2000 total scratches on a  $100 \text{ mm}$  diameter round substrate. The average relative velocity of the particle relative to the optic has been determined as  $80 \text{ cm/s}$ . Hence, for the length of scratches observed, the time that each of the rogue particles were loaded ranged between  $0.3$  and  $1.6 \text{ ms}$ . If we assume that the scratches were created randomly during the time of polishing of an hour, then a scratch is created on average every  $1.8$ – $24 \text{ s}$ . The conclusion here is that the scratching process occurs sporadically.

A longer scratch length suggests that rogue particle loads to the surface of the workpiece for a longer period of time, assuming a constant relative rogue particle velocity. In the discussion below, a mechanism is proposed by which the time for a rogue particle being loaded is governed by the size of the rogue particle and the viscoelastic properties of the lap. Fig. 12 shows a schematic of the proposed mechanism. At some arbitrary time zero, a rogue particle finds its way at the interface between the optic and the lap. Due to the large size of the rogue particle, it will bear a much higher load ( $P > 0.001 \text{ N}$ ) than the average particle on the lap; this load is sufficient to initiate a brittle fracture or plastic deformation on the optic. While loaded and static relative to the lap, the rogue particle will

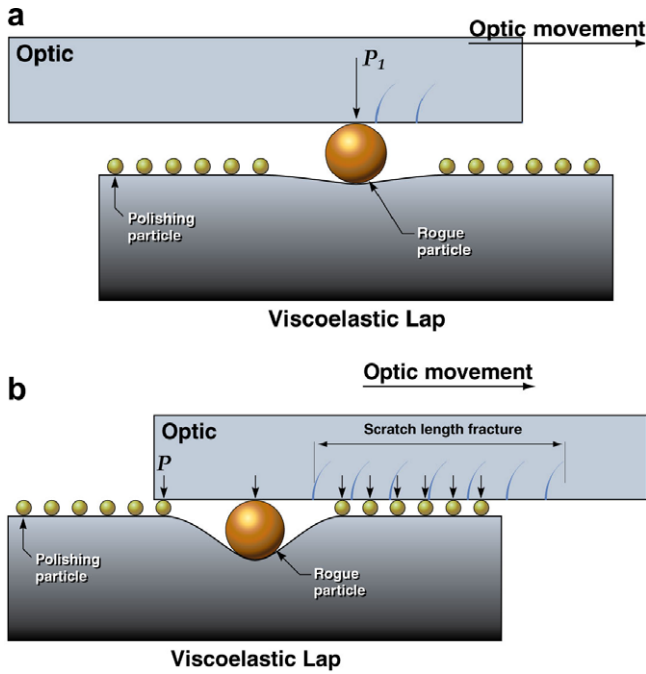


Fig. 12. Schematic of proposed mechanism for explaining the length of a scratch by a rogue particle on a viscoelastic lap.

penetrate into the viscoelastic lap until: (1) the gap between the lap and optic is reduced to that of the polishing ceria particle ( $0.5 \mu\text{m}$ ), thus dropping the load on the rogue particle to match that of the average ceria particle and ending the scratch (Fig. 12(b)), or (2) the maximum elastic penetration has been reached (function of the elastic modulus of the lap) resulting in incomplete rogue particle penetration, little drop in load on the rogue particles, and indefinite scratch lengths (across the length of the optic).

To examine this mechanism more quantitatively, consider a hard spherical abrasive under a quasi-static load (Fig. 13(a)). Using an approach Lee and Radock [19] which expanded the original Hertz elastic contact [20] to a simple linear viscoelastic substrate, the governing force balance equation is given by

$$E_{\text{Lap}}\varepsilon + \eta_{\text{Lap}} \frac{d\varepsilon}{dt} = \frac{P}{\pi a^2}, \quad (10)$$

where  $P$  is the applied load on the spherical particle,  $a$  is the contact zone radius, and  $\varepsilon$  is resulting strain. The viscoelastic properties of the lap are described by the elastic modulus ( $E_{\text{Lap}}$ ) and viscosity ( $\eta_{\text{Lap}}$ ). For a given applied pressure (term on right hand side of Eq. (10)), there is an elastic limit response (first term on left hand side) and a time dependent response (second term on left hand side).

One problem becomes immediately evident: most formulations are for small strain (i.e., small radius of contact compared to the radius of the particle). However, in this study we are interested in large strain. This problem has been noted by, for example, Kumar and Narasimhan [20]. The solution to this is to consider the shear strain so the strain variable is not  $a/R$  but

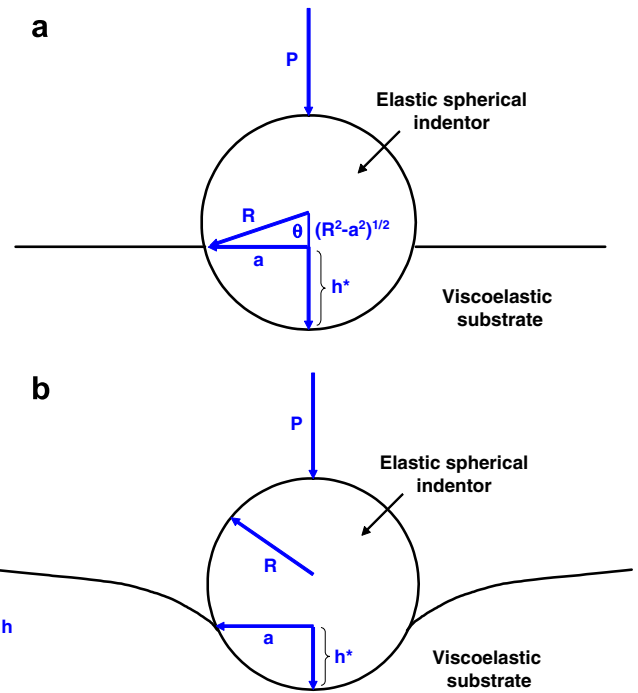


Fig. 13. Schematic illustrating the penetration of a hard spherical particle into a viscoelastic substrate (a) without surface displacement and (b) with surface displacement.

$$\varepsilon = \tan(\theta) = \frac{a}{\sqrt{R^2 - a^2}}, \quad (11)$$

where  $R$  is the radius of the particle and  $\theta$  is the angle between the contact zone edge and vertical plane running through the center of the particle. Combining Eqs. (10) and (11) and rewriting gives:

$$\frac{\partial \varepsilon}{\partial t} + \frac{E_{\text{Lap}}}{\eta_{\text{Lap}}} \varepsilon = \frac{P}{\pi R^2 \eta_{\text{Lap}}} \left( \frac{1 + \varepsilon^2}{\varepsilon^2} \right). \quad (12)$$

It is convenient to rewrite Eq. (12) using:

$$\chi = \varepsilon^3 = \frac{a^3}{(R^2 - a^2)^{3/2}}, \quad (13a)$$

$$\tau = \frac{\eta_{\text{Lap}}}{3E_{\text{Lap}}}, \quad (13b)$$

which results in:

$$\frac{\partial \chi}{\partial t} + \frac{\chi}{\tau} = \frac{3P}{\pi R^2 \eta_{\text{Lap}}} (1 + \chi^{2/3}). \quad (14)$$

Eq. (14) can be solved numerically and using Eqs. (13a&b), the contact zone as a function of time ( $a(t)$ ) can be solved.

However, the key parameter needed is the total penetration as a function of time. The penetration in reality has two components. The first component is the penetration depth ( $h^*$ ) due to the contact zone and the geometry of the particle (see Fig. 13(a)) with the result:

$$h^* = R - \sqrt{R^2 - a^2}. \quad (15)$$

The second component is due to the fact that the baseline surface is also displaced away from the contact zone (see Fig. 13(b)). Hunter [21] and Ting [22] have shown approaches to account for the surface displacement. Ting’s approach provides an analytical expression for the total displacement in terms of the contact zone radius and can be applied to high strain which is given by:

$$h(r, t) = \begin{cases} \frac{a(t)}{2} \ln \left( \frac{R+a(t)}{R-a(t)} \right) - \left( R - \sqrt{R^2 - r^2} \right) & \text{for } r < a \\ \left( a \ln \left( \frac{R+a(t)}{R-a(t)} \right) - 2R \right) \frac{\sin^{-1} \left( \frac{a(t)}{r} \right)}{\pi} + \frac{1}{\pi} \sqrt{r^2 - a(t)^2} \ln \left( \frac{R+a(t)}{R-a(t)} \right) - \frac{1}{\pi} \sqrt{r^2 - R^2} \ln \left( \frac{\sqrt{r^2 - a(t)^2} + \frac{R}{\pi} \sqrt{r^2 - R^2}}{\sqrt{r^2 - a(t)^2} - \frac{R}{\pi} \sqrt{r^2 - R^2}} \right) & \text{for } r > a, \end{cases} \quad (16)$$

where  $r$  is radial distance away from the center of the particle.

Now consider a rogue particle penetrating into the lap as described in Fig. 13. The particle would penetrate until the load subsides in the part and has essentially penetrated a distance:

$$h_f = 2(R - R_{\text{base}}). \quad (17)$$

Hence a 4  $\mu\text{m}$  rogue particle will at most penetrate 3.5  $\mu\text{m}$ , because the diameter of the Ceria slurry is 0.5  $\mu\text{m}$ . The total penetration as a function of time can now be calculated using Eqs. (13a), (14) and (16). Using the known properties of the polyurethane pad ( $E = 100 \text{ MPa}$ ;  $\eta = 9 \times 10^7 \text{ Poise}$ ) [23], and assuming a load of 1 N (in the range needed to cause brittle scratches), the penetration of the rogue particle as a function of time was calculated for samples P3, and P6–P9. The results are shown in Fig. 14(a). The model predicts penetration times that are longer for larger rogue particles. For the rogue particles in the range 4–20  $\mu\text{m}$  penetration times of 1–5 ms are calculated. Both of the above results are consistent with the experimental data.

Notice in Fig. 14(b) that the 45  $\mu\text{m}$  particle does not completely penetrate at low loads. It is useful to consider a figure-of-merit (FOM) which would determine if a spherical particle would reach an equilibrium depth or penetrate the diameter of the rogue particle. Consider the case where the particle reaches equilibrium, the strain rate in Eqs. (12) or (14) goes to zero. Rewriting gives an expression for the equilibrium strain ( $\epsilon_\infty$ ) as

$$\frac{\epsilon_\infty^3}{1 + \epsilon_\infty^2} = \frac{P}{\pi R^2 E}. \quad (18)$$

Rewriting Eq. (11) gives an expression for the equilibrium contact zone  $a_\infty$

$$\frac{a_\infty}{R} = \sqrt{\frac{\epsilon_\infty^2}{1 + \epsilon_\infty^2}}. \quad (19)$$

Similarly, the equilibrium penetration ( $h_\infty$ ) can then be determined in terms of  $a_\infty$  using Eq. (16) evaluated at  $r = 0$ :

$$\frac{h_\infty}{R} = \frac{a_\infty}{2R} \ln \left( \frac{1 + \frac{a_\infty}{R}}{1 - \frac{a_\infty}{R}} \right). \quad (20)$$

By combining Eq. (18)–(20), the equilibrium penetration is solely dependent on the stress parameter ( $\alpha = \frac{P}{\pi R^2 E}$ ) on the right hand side of Eq. (18). Fig. 15(a) shows a plot of equilibrium strain ( $\epsilon_\infty$ ), normalized equilibrium contact zone

( $a_\infty/R$ ), and the normalized equilibrium penetration ( $h_\infty/R$ ) as a function of stress parameter ( $\alpha$ ) calculated using Eqs. (18)–(20). This set of global curves shows the equilibrium condition at long times. For the specific case of the rogue particles, the rogue particle will bear the large load until it penetrates roughly the diameter of the particle. In

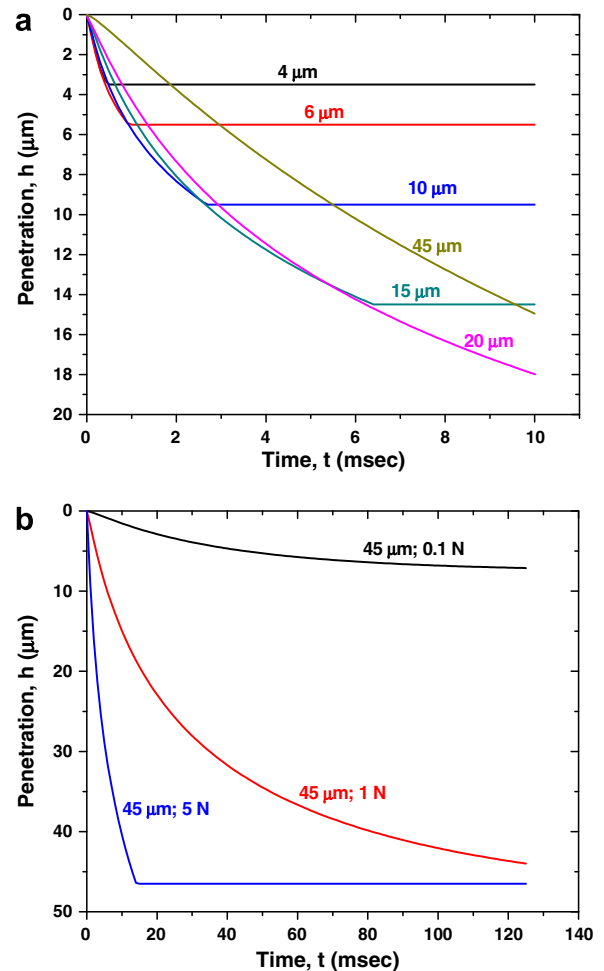


Fig. 14. (a) Calculated depth of particle penetration using Eqs. (10)–(12), (13a), (13b), (14)–(17) as a function of time for different size rogue diamond particles at a load of 1 N. (b) Calculated depth of particle penetration using Eqs. (10)–(12), (13a), (13b), (14)–(17) as a function of time for different loads.

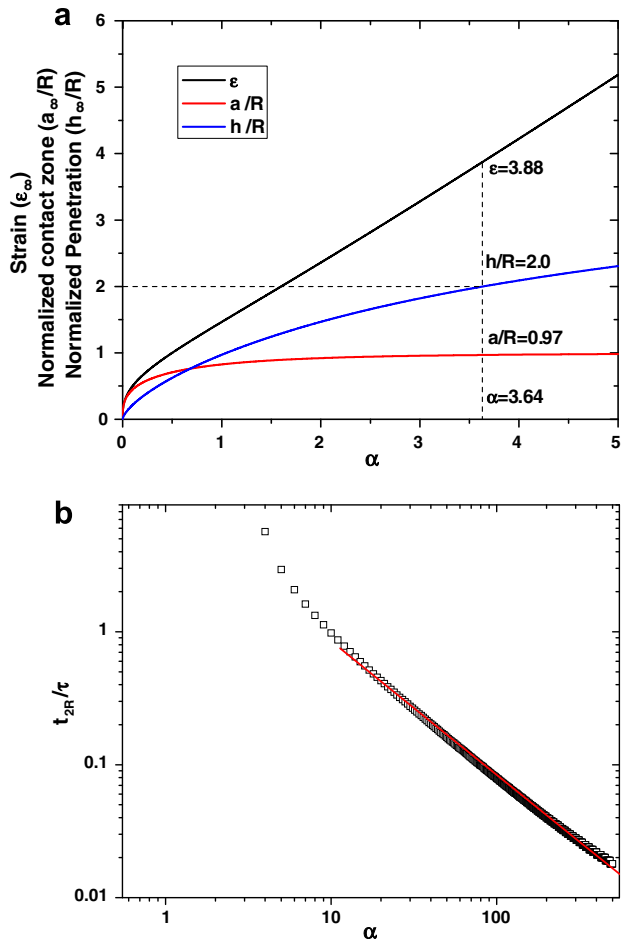


Fig. 15. (a) Calculated equilibrium strain ( $\epsilon_\infty$ ), normalized contact zone ( $a_\infty/R$ ), and penetration ( $h_\infty/R$ ) as a function of the stress parameter ( $\alpha$ ); (b) calculated normalized time for complete particle penetration of a rogue particle into the lap at a critical strain of 3.88 as function of the stress parameter ( $\alpha$ ). The line in (b) represents a single exponential fit to the calculation for  $\alpha > 4$ .

other words, this is until  $h/R \sim 2$  (for cases where the rogue particle radius  $\geq$  base particle radius). This point is reached when the stress parameter reaches a value of 3.64. Hence for values of the load parameter greater than 3.64, the particle will reach its maximum penetration; for values of  $\alpha < 3.64$ , an equilibrium penetration will be reached before full penetration of the particle. In the latter case, the scratch length will always be infinite. Another interesting point is that at an  $\alpha$  of 3.64, the strain will be 3.88 and the normalized contact zone will be 0.97.

The analysis described above can be used to establish a more simple, time dependent solution for the case of the rogue particle. Rewriting Eq. (14) in terms of  $\tau$  and  $\alpha$  one finds

$$\frac{\partial \chi}{\partial t} + \frac{\chi}{\tau} = \frac{\alpha}{\tau} (1 + \chi^{2/3}). \tag{21}$$

The solution to Eq. (21), evaluated at the maximum strain of 3.88 is shown in Fig. 15b. This plot which is portrayed as normalized time vs load parameter is a global plot to deter-

mine the time of penetration of a rogue particle for given load, particle size, and lap properties (viscosity, modulus). When  $\alpha$  is increased (higher loads and/or smaller particles), the time for penetration decreases. Although this plot was determined numerically, this global plot can be described analytically by the following simple expression:

$$\log(t_{2R}) \cong -\log(\alpha) + 0.93, \tag{22a}$$

for values of  $\alpha$  greater than 4. Rewriting in terms of scratch length and material parameters gives

$$\langle L_s \rangle \cong 8.9 \frac{\langle v \rangle \eta R^2}{P}, \tag{22b}$$

where  $\langle v \rangle$  is the average relative velocity of the particle relative to the optic surface. Using Eq. (22b) or by performing the numerical calculation of Eqs. (18)–(20), the crack lengths were calculated at loads of 1 N and 5 N (in the range needed to cause scratches) and compared to the measured scratch lengths in Fig. 16 as a function of rogue particle size. The bars in the measured data represent 80% of the distribution of scratch lengths observed. Note that the data is bound within the load range of 1–5 N. Also, the stress parameter value of 3.64 is reached at a nominal size of 30  $\mu\text{m}$  for a load of 1 N. Above this size, the model predicts infinitely long scratches (i.e. scratch lengths extending to the edge of the workpiece); again consistent with the experimental data where the 45  $\mu\text{m}$  particles led to infinitely long scratches. Eq. (22b) serves as a simple expression that can be used to determine the length of the scratch based on the size of the rogue particle, load, kinematic and material properties of the lap.

The validity of the viscoelastic mechanism for explaining scratch length can be examined semi-quantitatively by plotting the scratch length not only as a function of rogue particle size, but as a function of a number of other parameters such as lap viscosity (determined either by temperature or lap material used) or and applied pressure. These results

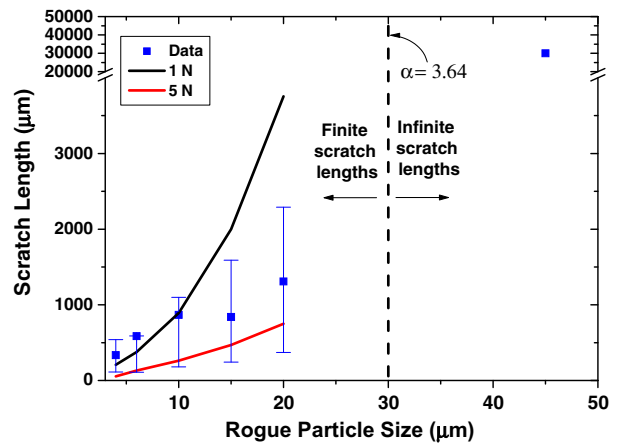


Fig. 16. Average scratch length measured as a function of rogue particle size (same data shown in Fig. 9(c)) compared with the simple viscoelastic model at two different loads of 1 N and 5 N. Note the bars on the data point represent the 80% of the distribution of scratch lengths observed.

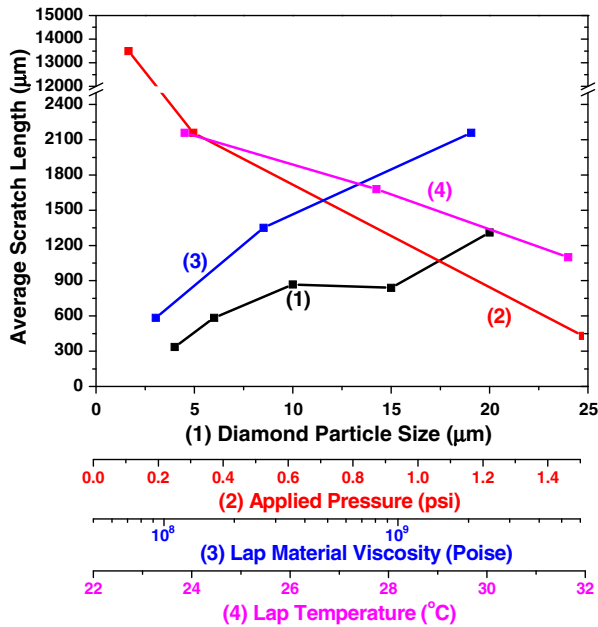


Fig. 17. Average scratch length measured as a function of system variables explored in this study (diamond particle size (P3, P6–P9); applied pressure (P11–13); lap material (P12, P15–P16); Lap (pitch) temperature (P11–P13)).

are summarized in Fig. 17 and in Table 2. In the case for the lap material (Suba 550, IC1000, or Pitch), the scratch length was observed to increase with increase in lap viscosity. Also, the temperature of the lap influenced the scratch length. As the temperature was increased, the lap viscosity decreased and scratch length decreased. Finally, as the applied pressure was increased, the scratch length was found to decrease. All of these trends are consistent with the viscoelastic mechanism for explaining scratch lengths.

## 5. Conclusions

The distribution and characteristics of surface cracking (i.e., sub-surface damage or SSD) formed during grinding and polishing fused silica glass in the presence of rogue particles (i.e. larger particles than the mean size of the nominal grinding/polishing media) was investigated. The addition of rogue particles during grinding revealed that a small amount of rogue particles ( $>10^{-4}$  rogue fraction) is enough to noticeably increase both the SSD depth and the removal rate. The addition of rogue particles during polishing revealed that: (1) the efficiency by which rogue particles can lead to scratching is strongly dependent on the size of the rogue particle and weakly dependent on the concentration for most of the rogue concentrations; (2) the length and width of the scratches both increase with the size of the

rogue particle and are essentially independent of the rogue particle concentration; (3) at the highest rogue particle size (45 µm) and at the very high rogue concentrations for the 4 µm diamond, the number density of scratches increases by orders of magnitude, the scratch lengths are the length of the optic (quasi infinite) and the nature of the scratches are all plastic in nature. The latter two effects are well described using a simple model which relies on the time needed for rogue particle penetration into a viscoelastic lap. A simple relation resulting from the model (Eq. (22b)) allows one to estimate the scratch length based on the viscoelastic properties of the lap and size of the rogue particle.

## Acknowledgements

Work performed under the auspices of the US Department of Energy by Lawrence Livermore National Laboratory under Contract No. W-7405-ENG-48 with the LDRD program. The authors would like to thank Ed Lindsey for SEM images of the diamond particles.

## References

- [1] G. Beilby, *Aggregation and Flow of Solids*, Macmillan & Co., London, 1921.
- [2] L. Cook, *J. Non-Cryst. Solids* 120 (1990) 152.
- [3] L. Samuels, *Metallographic Polishing by Mechanical Methods*, 2nd ed., Elsevier, New York, 1971.
- [4] B. Lawn, *Fracture of Brittle Solids*, 2nd Ed., Cambridge Solid State Science Series, 1993.
- [5] I. Hutchings, *Tribology: Friction and Wear of Engineering Materials*, Butterworth/Heinemann, 1992.
- [6] E. Rabinowicz, *Sci. Amer.* 218 (1968) 91.
- [7] R. Komanduri, D. Lucca, Y. Tani, *Ann. CIRP* 46 (1997) 545.
- [8] Q. Lou, S. Ramarajan, S. Babu, *Thin Solid Films* 335 (1998) 160.
- [9] M. Swain, *Proc. R. Soc. London A* 366 (1979) 575.
- [10] K. Li, W. Liao, *J. Mater. Proc. Technol.* 57 (1996) 207.
- [11] Y. Ahn, J. Yoon, C. Baek, Y. Kim, *Wear* 257 (2004) 785.
- [12] G. Basim, J. Adler, R. Singh, B. Moudgil, *J. Electrochem. Soc.* 147 (9) (2000) 3523.
- [13] C. Kallingal, D. Duquette, S. Murarka, *J. Electrochem. Soc.* 145 (6) (1998) 2074.
- [14] T. Suratwala, L. Wong, P. Miller, M. Feit, J. Menapace, R. Steele, P. Davis, D. Walmer, *J. Non-Cryst. Sol.* 352 (2006) 5601.
- [15] J. Menapace, P. Davis, L. Wong, W. Steele, T. Suratwala, P. Miller, *SPIE 5991, Boulder Damage Symposium XXXVII* (2005).
- [16] P. Miller, T. Suratwala, L. Wong, M. Feit, J. Menapace, P. Davis, R. Steele, *SPIE 5991, Boulder Damage Symposium XXXVII* (2005).
- [17] M. Feit, A. Rubenchik, *SPIE 5273* (2003) 264.
- [18] F. Preston, *Trans. Opt. Soc.* 23 (3) (1922) 141.
- [19] E.H. Lee, J.R.M. Radok, *J. Appl. Mech.* (September) (1960) 438.
- [20] M. Oyen, *J. Mater. Res.* 20 (August) (2005) 2094.
- [21] S.C. Hunter, *J. Mech. Phys. Solids* 8 (1960) 219.
- [22] T.C.T. Ting, *Trans. ASME J. Appl. Mech.* 33 (1966) 845.
- [23] Values from H. Lu, *Mater. Characterization* 49 (2003).